Effect of annealing on the damage threshold and optical properties of $HfO_2/Ta_2O_5/SiO_2$ high-reflection film

Jianing Dong (董家宁), Jie Fan (范 杰)*, Sida Mao (毛思达), Yunping Lan (兰云萍), Yonggang Zou (邹永刚), Haizhu Wang (王海珠), Jiabin Zhang (张家斌), and Xiaohui Ma (马晓辉)

State Key Laboratory of High-Power Semiconductor Laser, Changchun University of Science and Technology, Changchun 130022, China

**Corresponding author: fanjie@cust.edu.cn*

Received May 7, 2019; accepted July 5, 2019; posted online September 9, 2019

The effect of thermal annealing on the optical properties, microstructure, and laser-induced damage threshold (LIDT) of $HfO_2/Ta_2O_5/SiO_2$ HR films has been investigated. The transmission spectra shift to a short wavelength and the X-ray diffraction peaks of monoclinic structure HfO_2 are enhanced after thermal annealing. The calculated results of the m(−111) diffraction peak show that the HfO_2 grain size is increased, which is conducive to increasing the thermal conductivity. Thermal annealing also reduces the laser absorption of high-reflection films. The improvement of thermal conductivity and the decrease of laser absorption both contribute to the improvement of LIDT. The experimental results show that the highest LIDT of 22.4 J/cm^2 is obtained at 300°C annealing temperature. With the further increase of annealing temperature, the damage changes from thermal stress damage to thermal explosion damage, resulting in the decrease of LIDT.

OCIS codes: 310.1620, 310.4165, 310.4925.
doi: 10.3788/COL201917.113101.

Since Ta_2O_5 has the characteristics of low intrinsic stress, superior layer smoothness and uniformity, and low absorption and scattering losses[1,2], the high-reflectivity (HR) films composed of Ta_2O_5 and SiO_2 have been widely used in various optical systems. As the output power of optical system increases steadily, HR films are expected to have a higher laser-induced damage threshold (LIDT) to ensure the stability and security characteristics of optical systems. However, the lower LIDT of Ta_2O_5/SiO_2 HR films caused by the low laser damage resistance of Ta_2O_5 results in films damaged easily, which affects the stability and security of the optical system. Since damage usually occurs on the outermost layers of HR films due to the high laser energy suffered here, the LIDT of HR films can be effectively improved by replacing the outermost layers with high LIDT materials. In order to improve LIDT of Ta_2O_5/SiO_2 HR films, Patel *et al.*[3] replaced the outermost three Ta_2O_5 layers by HfO_2 and formed $HfO_2/Ta_2O_5/SiO_2$ HR film, increasing the LIDT of HR film from 16 J/cm^2 to 25 J/cm^2. Schiltz *et al.*[4] replaced the outermost Ta_2O_5 layers of Ta_2O_5/SiO_2 HR film with HfO_2, and the LIDT of HR film increased by nearly three times. Despite the great improvements made in Ta_2O_5/SiO_2 HR film by replacing Ta_2O_5 with HfO_2, the LIDT of $HfO_2/Ta_2O_5/SiO_2$ films is expected to be further improved. As one of the post-treatment technologies of film, thermal annealing can effectively improve the laser damage resistance of HR films. The LIDT is mainly affected by the oxygen vacancies, nodule, impurity, microstructural and mechanical properties of HR films in the nanosecond pulse regime. Thermal annealing can improve microstructures and reduce the oxygen vacancies by providing thermal energy[5,6]. Zhao *et al.*[7] show that thermal annealing can increase the LIDT of Ta_2O_5/SiO_2 dielectric mirrors by improving the structure and absorbance. The roles of thermal annealing on the LIDT of HR films are different according to the annealing temperature and process. Xu *et al.*[8] studied the effect of high-temperature annealing on Ta_2O_5 films and obtained the maximal LIDT at 873 K annealing temperature. Bananej *et al.*[9] studied the effect of the annealing processes on the properties of ZrO_2 thin films and found that the time–temperature gradient annealing can obtain higher LIDT. Hassanpour *et al.*[10] realized the enhancement of LIDT of TiO_2 by using the same method. Film stress can be changed by thermal annealing. Shen *et al.*[11] showed that the residual stress of HfO_2/SiO_2 film is compressive at as-deposited and transforms into tensile after annealing at 200°C; the thin film even appears with microcracks at 400°C, which seriously affect the LIDT. Jena *et al.*[12] found that the LIDT of HfO_2/SiO_2 film can be increased when thermal annealing temperature is below 400°C. The HR films annealed at 400°C show the highest LIDT and an increase of 74% compared to the as-deposited HR films.

To our best knowledge, there are few reports about the effect of thermal annealing on LIDT of $HfO_2/Ta_2O_5/SiO_2$ HR films. In the present study, thermal annealing is adopted to improve $HfO_2/Ta_2O_5/SiO_2$ HR films that are prepared by electron beam evaporation with ion beam assisting. The optical properties, microstructure, and nanosecond LIDT of $HfO_2/Ta_2O_5/SiO_2$ HR films annealed at different temperatures are comparatively investigated. The experimental results show that the highest LIDT

of 22.4 J/cm^2 is obtained at 300°C annealing temperature. With the further increase of annealing temperature, the damage changes from the delamination phenomenon to the craters phenomenon, and the effect of thermal annealing on the damage mechanism of the HR film is analyzed by damage morphology.

The HR films are deposited by electron beam evaporation (Leybold Optics, ARES710, Germany) with ion beam assisting on BK7. The structure of HR film is $|(LH)^{\hat{8}}(LM)^{\hat{3}}|$ air, where L, M, and H stand for SiO_2 layers, HfO_2 layers, and Ta_2O_5 layers, respectively. The thickness of the SiO_2 layer is 170 nm, and the thickness of the HfO_2 layer is 124 nm. For the four Ta_2O_5 layers near HfO_2, the thickness of each layer is 124.5 nm. The thickness of the remaining Ta_2O_5 layer is 129 nm. In this HR film structure, the maximum electric field is located at the top HfO_2 layer. A quartz crystal monitor is used to measure deposition rate and layer physical thickness. The initial pressure of the coating chamber is 8×10^{-6} mbar, and the temperature of substrate is 100°C. The deposition rates of HfO_2 and Ta_2O_5 layers remain at 0.2 nm/s, while that of the SiO_2 layer is 0.6 nm/s. Table 1 shows the ion source parameter during deposition in detail. The thermal annealing post-process is performed at 200°C, 300°C, 400°C, and 500°C for 3 h in the furnace with the air environment. The heating rate is 5°C/min, and the temperature falls naturally to room temperature in the furnace after thermal annealing.

A spectrophotometer (Shimaszu, UV-3101, Japan) is used to measure the transmission spectra of the HR films from 800 nm to 1400 nm, and the relative uncertainty in the transmittance is 0.3%. The transmission spectra of the HR films at different annealing temperatures are shown in Fig. 1. In the range of 950 nm to 1110 nm, all HR films have a transmittance of less than 1%. With the annealing temperature increasing to 500°C, the spectra of the HR film shift to a short wavelength. The inset of Fig. 1 shows the transmission spectra from 1250 nm to 1290 nm in detail. The transmission peak of the as-deposited HR film is at 1275 nm, and it moves to 1266 nm when the annealing temperature rises to 500°C. The short wavelength shift of the transmission spectra indicates that the layers of HR films become thinner and more compact.

The spectral shift to a short wavelength can be explained by the fact that the atoms of HR films are activated to fill the voids and diffuse into each layer in the process of thermal annealing[13]. The decrease of the void

Table. 1. Ion Source Parameter during Deposition

Material	Anode Voltage (V)	O_2 (sccm[a])	Ar (sccm[a])
SiO_2	160	5	5.5
Ta_2O_5	150	5	5
HfO_2	150	5	5

[a]sccm, standard cubic centimeters per minute.

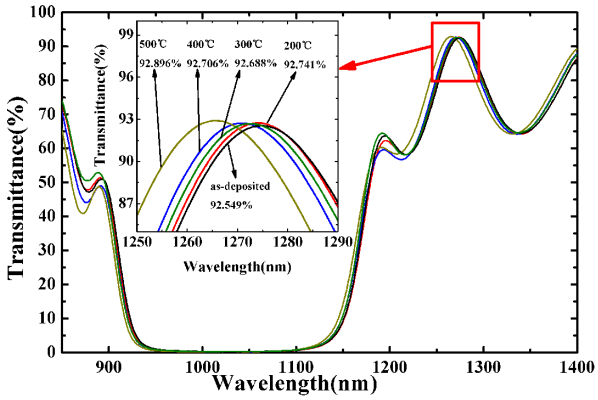

Fig. 1. Transmission spectra of the HR films at different annealing temperatures.

density reduces the layer physical thickness, which leads to the decrease of the optical thickness, resulting in the shift of the transmission spectra to a short wavelength.

Due to the fact that the maximum electric field is located at the top HfO_2 layer, the LIDT of the HR film is mainly affected by the top HfO_2 layer. Electron beam evaporation introduces nonstoichiometric hafnium oxide and oxygen vacancies[14]. The oxygen deficiency enhances the absorption of films and decreases the band gaps, which seriously decrease the LIDT[15]. The existence of oxygen vacancies increases the concentration of free electrons, which affect the absorption coefficient. The relationship between the absorption coefficient α and the concentration of free electrons N can be expressed as[12]

$$\alpha = \frac{Ne^2\lambda^2}{mn\tau\varepsilon_0\pi^2c^3}, \tag{1}$$

where e, n, m, τ, λ, and ε_0 are the charge of the electron, refractive index, mass of the free electron, relaxation time, absorption wavelength, and vacuum permittivity, respectively. During thermal annealing, oxygen atoms react with the nonstoichiometric hafnium oxide, thus gradually reducing the oxygen vacancies and the concentration of free electrons N.

Equation (1) indicates that the absorption coefficient α is not only related to oxygen vacancies but is also affected by the refractive index. The refractive index of HfO_2 also changes during thermal annealing. In order to clarify the effect of thermal annealing on the refractive index of HfO_2, the HfO_2 single layer film is fabricated with the same parameter as HR films. The process of thermal annealing is the same as that of the HR film. The refractive index of HfO_2 at different annealing temperatures is obtained from the transmittance spectrum by using the envelope method and Essential Macleod software[16]; the relative uncertainty in the refractive index is about 1.3%. Figure 2 shows the influence of the annealing temperature on the refractive index of HfO_2 at 550 nm. The refractive index is increased slightly with increasing annealing temperatures, which had also been observed in TiO_2[17].

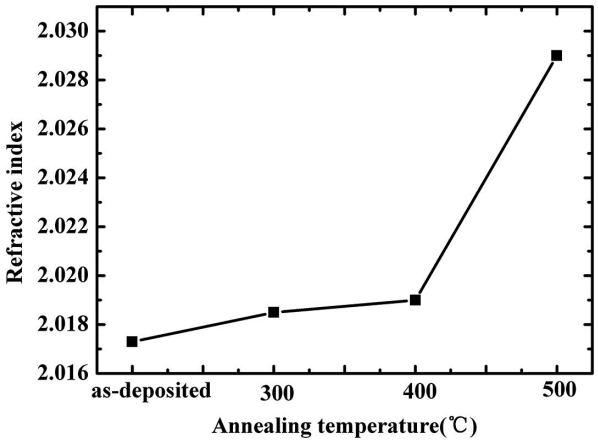

Fig. 2. Influence of annealing temperature on refractive index of HfO_2 at 550 nm.

The reduction of oxygen vacancies and the increase of the refractive index both decrease the absorption coefficient of the top HfO_2 layer. Since the LIDT of HR films is inversely proportional to the absorption coefficient[18], reducing the absorption coefficient contributes to the improvement of LIDT.

Decreasing the layer physical thickness and increasing the refractive index indicate that the density (ρ_{film}) of the film is increased[19]; the increasing densities are beneficial to improving the damage threshold of thin films by decreasing the porosity of film and increasing the specific heat. Based on the defect originated thermal damage mechanism, the LIDT is proportional to the 1/2 power of the density, which can be expressed as[19]

$$E_T \approx \frac{16\,T_C}{\pi}(\rho_{\text{film}} c_{\text{film}} k_{\text{film}} \tau)^{1/2}, \tag{2}$$

where E_T, T_C, ρ_{film}, c_{film}, τ, and k_{film} are the damage threshold in joules per square centimeter, the critical temperature (e.g., melting temperature of the host film material), the density of the host, the effective specific heat at constant pressure of the host, the laser pulse length, and the thermal conductivity of the host material, respectively. In addition, thermal annealing can also remove adsorbed water, hydrocarbons, and carbon in HR films, thereby reducing the absorption laser energy ability of the HR film.

The microstructure of HR films is investigated by X-ray diffraction (XRD) with a 2θ angle in the range of 15°–65° using Cu–Kα radiation at the wavelength of 1.54 Å (1 Å = 0.1 nm). The measured XRD patterns are shown in Fig. 3. Since Ta_2O_5 and SiO_2 are amorphous when the annealing temperature is below 500°C[8,12], the XRD peaks in Fig. 3 can be considered to belong to HfO_2.

For the as-deposited HR film, the most remarkable diffraction peak is at $2\theta = 28.36°$, and there are several weak diffraction peaks nearby. According to the probability density function (PDF) card (PDF#00-006-0318), the diffraction peak at 28.36° corresponds to the m(−111) plane

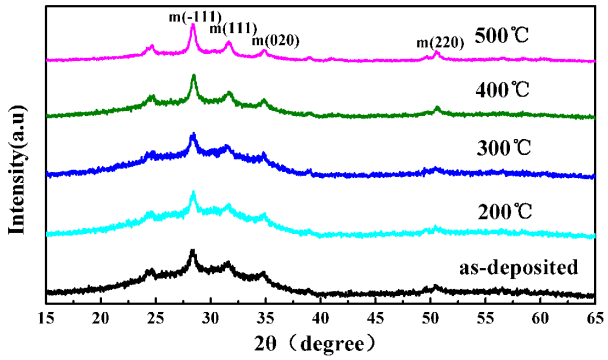

Fig. 3. XRD spectra of $HfO_2/Ta_2O_5/SiO_2$ HR films at different annealing temperatures.

of monoclinic structure HfO_2, and the other diffraction peaks correspond to the m(111) plane, m(020) plane, and m(220) plane, respectively. After thermal annealing, the intensity of all diffraction peaks is enhanced, and no new diffraction peak appears. The enhancement of diffraction peak intensity indicates that the crystallinity of the HfO_2 is improved. The HfO_2 crystallite size c_{HfO2} can be calculated by the HfO_2 m(−111) diffraction angle θ and the full width at half-maximum (FWHM) of diffraction peaks according to Scherer's formula[20]:

$$c_{\text{HfO}_2} = \frac{0.89\lambda_{\text{XRD}}}{\beta \cos\theta}, \tag{3}$$

where β is the FWHM of the diffraction peak, and λ_{XRD} is 0.154 nm, which is dependent on the XRD equipment. The calculated results for the m(−111) plane of monoclinic structure HfO_2 are shown in Fig. 4.

The HfO_2 crystallite size is increased with increasing annealing temperature. When the annealing temperature is below 300°C, the crystallite size increases slightly with the increase of annealing temperature. The crystallite size increases from 12.18 nm of the as-deposited HR film to 12.74 nm at 300°C. With annealing temperature

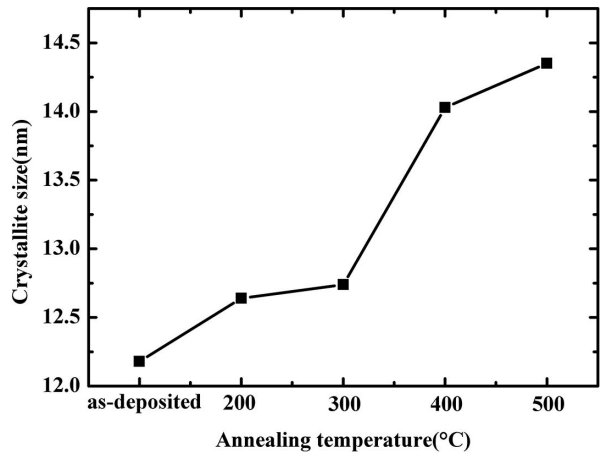

Fig. 4. Influence of annealing temperature on HfO_2 crystallite size in the HR films.

exceeding 300°C, the crystallite size increases rapidly with the increase of annealing temperature. The crystallite size increases to 14.03 nm when the HR film is annealed at 400°C and to 14.35 nm at 500°C. The change of crystallite size reflects the change of grain size. It is the fact that the process of thermal annealing can restore and recrystallize the microstructure of HR films. When the annealing temperature is below 300°C, the thermal energy offered by annealing is mainly used to restore the microstructure of HR film, and thus the grain size of HR films changes indistinctively. As the annealing temperature is further improved, in addition to repairing the HR film microstructure, thermal annealing can provide more thermal energy to promote grain size growth. Thus, when the annealing temperature is higher than 400°C, the grain size of the HR film increases significantly. The increase of grain size increases the average free path of phonon scattering at grain boundaries and decreases the thermal boundary impedance[21,12], which helps to improve the thermal conductivity of $HfO_2/Ta_2O_5/SiO_2$ HR films.

Thermal conductivity is a key factor affecting the laser resistance of HR films. The improved thermal conductivity of films not only effectively suppresses temperature rises in the laser irradiation area by transferring generated heat away, but also increases the laser-induced thermal stress resistance factor[22]. Equation (2) indicates that the LIDT is proportional to the 1/2 power of the thermal conductivity. Therefore, the LIDT can be increased by improving thermal conductivity.

The LIDTs of HR films are measured in the "one-on-one" regime according to the International Organization for Standardization (ISO) standard 11254-1[23], where a 1064 nm pulsed laser at a pulse width of 12 ns is used to assess the LIDTs. The damage threshold error is about 11%. The influence of the annealing temperature on the LIDT of HR films is shown in Fig. 5. As can be seen from the figure, the LIDTs increase with the increase of annealing temperature when the thermal annealing temperature is below 300°C. The LIDT of HR films reaches the highest value of 22.4 J/cm^2 at the annealing temperature of 300°C, which is twice as high as that of the as-deposited HR film.

However, when the annealing temperature exceeds 400°C, the LIDT decreases with the increase of annealing temperature, and the LIDT is 9.5 J/cm^2 at 500°C, which is lower than that of as-deposited HR film.

$HfO_2/Ta_2O_5/SiO_2$ HR films are irradiated by the energy density of 25.5 J/cm^2. The damage morphologies of the films are observed by a metallographic microscope with magnification of 500 times, and the results are shown in Fig. 6. The damage morphologies of HR film are

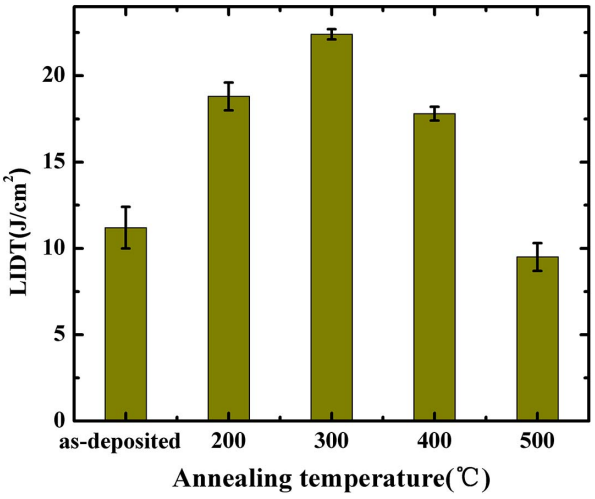

Fig. 5. Influence of annealing temperature on LIDT of HR films.

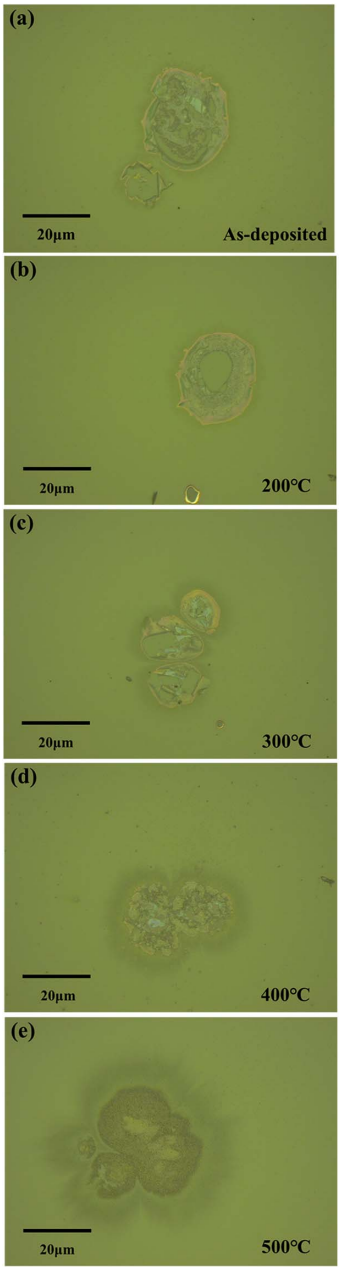

Fig. 6. Damaged morphologies of HR films under the laser energy density of 25.5 J/cm^2.

obviously different at different annealing temperatures, which indicate that the causes of damage factors have changed.

The damaged morphologies are similar when annealing is below 300°C. The damage morphologies are captured by delamination, and there are membranes warping at the edge of the damage; the boundary of damaged areas and undamaged areas is distinct. The delamination phenomenon of HR films is mainly caused by thermal stress. The temperature rises sharply at the laser spot center and forms a temperature difference with the surroundings. Thermal expansion caused by temperature difference eventually produces thermal stress in the film. The relationship between thermal stress and temperature difference can be written as[22]

$$\sigma = \frac{\eta E}{3(1-2\nu)} \Delta T, \tag{4}$$

where σ represents the thermal stress of HfO_2 thin films, η is the thermal expansion coefficient of HfO_2 films, E is the elastic modulus of HfO_2, ν represents the Poisson ratio of HfO_2, and ΔT is the temperature difference of the film produced by laser irradiation. When the thermal stress σ reaches the critical stress value, damage occurs in HR films, and delamination is formed. The delaminated damage in the HR film is observed when annealing is below 300°C. The improvement of LIDT of $HfO_2/Ta_2O_5/SiO_2$ can be attributed to the decrease of the absorption coefficient and the increase of thermal conductivity and density.

When the annealing temperature exceeds 400°C, the damage morphologies are the craters with broken spots, the edges of damaged areas are surrounded by ablation pattern, and the surface roughness of the damaged area is increased. The boundary of damaged areas and undamaged areas is blurred. This denotes that the damage is mainly caused by thermal explosion. Thermal explosion is caused by defects points, including inclusions, nodules, nonstoichiometric defects, and particles. For particles, when the film becomes too dense, the particles will exert pressure on the film. Under laser irradiation, the temperature of particles introduced in the preparation will increase sharply. High temperature results in vaporization of film material around particles and generates high-temperature plasma. The high temperature plasma continues to heat up and produces shock waves in subsequent laser irradiation, finally breaking through the bondage of the film layer and producing thermal explosion damage. After high temperature thermal annealing, the $HfO_2/Ta_2O_5/SiO_2$ HR films become denser. The thermal expansion of impurity particles in the HR film is limited, resulting in a high-pressure exertion on the film. The laser damage thus occurs easier[24,25]. Therefore, when the annealing temperature is higher than 400°C, the LIDT of the HR film decreases with the increase of annealing temperature, and it decreases sharply to 9.5 J/cm^2 at 500°C.

In this Letter, the optical properties, microstructure, and LIDT of $HfO_2/Ta_2O_5/SiO_2$ HR films at different annealing temperatures have been studied. After thermal annealing, the spectra of the HR film shift to a short wavelength, and the grain size of HfO_2 is increased. With the increase of annealing temperature, the LIDT of the HR films is increased due to the increase of thermal conductivity and decrease of the absorption coefficient. The LIDT of the HR film reaches 22.4 J/cm^2 at the annealing temperature of 300°C, which is twice as high as that of the films without the annealing treatment. However, when the annealing temperature exceeds 400°C, the damage changes from thermal stress to thermal explosion, resulting in a sharp decrease in LIDT, and the LIDT is only 9.5 J/cm^2 at 500°C, which is lower than that of the as-deposited HR film.

This work was supported by the Jilin Science and Technology Development Plan (Nos. 20180519018JH and 20190302052GX), the Jilin Education Department "135" Science and Technology (No. JJKH20190543KJ), the National Natural Science Foundation of China (No. 11474038), and the Excellent Youth Foundation of Jilin Province (No. 20180520194JH).

Reference

1. S. G. Yoon, Y. T. Kim, H. K. Kim, M. J. Kim, H. M. Lee, and D. H. Yoon, Mater. Sci. Eng. B **118**, 234 (2005).
2. W. Kulisch, D. Gilliland, G. Ceccone, H. Rauscher, L. Sirghi, P. Colpo, and F. Rossi, J. Vac. Sci. Technol. A **26**, 991 (2008).
3. D. Patel, D. Schiltz, P. F. Langton, L. Emmert, L. N. Acquaroli, C. Baumgarten, B. Reagan, J. J. Rocca, W. Rudolph, A. Markosyan, R. R. Route, M. Fejer, and C. S. Menoni, Proc. SPIE **8885**, 888522 (2013).
4. D. Schiltz, D. Patel, L. Emmert, C. Baumgarten, B. Reagan, W. Rudolph, J. J. Rocca, and C. S. Menoni, in *Advanced Photonics* (2015), paper NS4B.3.
5. C. Xu, H. C. Dong, J. Y. Ma, Y. X. Jin, J. D. Shao, and Z. X. Fan, Chin. Opt. Lett. **6**, 228 (2008).
6. C. Wang, Y. Jin, D. Zhang, J. Shao, and Z. Fan, Opt. Laser Technol. **41**, 570 (2009)
7. Y. Zhao, Y. Wang, H. Gong, J. Shao, and Z. Fan, Appl. Surf. Sci. **210**, 353 (2003).
8. C. Xu, Q. Xiao, J. Ma, Y. Jin, J. Shao, and Z. Fan, Appl. Surf. Sci. **254**, 6554 (2008).
9. A. Bananej and A. Hassanpour, Appl. Surf. Sci. **258**, 2397 (2012).
10. A. Hassanpour and A. Bananej, Optik **124**, 35 (2013).
11. Y. Shen, Z. Han, J. D. Shao, S. Y. Shao, and H. B. He, Chin. Opt. Lett. **6**, 225 (2008).
12. S. Jean, R. B. Tokas, K. D. Rao, S. Thakur, and N. K. Sahoo, Appl. Opt. **55**, 1 (2016).
13. S. Jena, R. B. Tokas, S. Thakur, and N. K. Sahoo, AIP Conf. Proc. **1832**, 060005 (2017).
14. J. Ni, Q. Zhou, Z. Li, and Z. Zhang, Appl. Phys. Lett. **93**, 011905 (2008).
15. C. Xu, P. Yi, H. Fan, J. Qi, Y. Qiang, J. Liu, C. Tao, and D. Li, Appl. Surf. Sci. **289**, 141 (2014).
16. R. Swanepoel, J. Phys. E: Sci. Instrum. **16**, 1214 (1983).
17. J. Yao, J. Shao, H. He, and Z. Fan, Appl. Surf. Sci. **253**, 8911 (2007).
18. D. Zhang, J. Shao, D. Zhang, S. Fan, T. Tan, and Z. Fan, Opt. Lett. **29**, 2870 (2004).

19. S. Jena, R. B. Tokas, S. Tripathi, K. D. Rao, D. V. Udupa, S. Thakur, and N. K. Sahoo, J. Alloy Compd. **771**, 373 (2019).
20. A. L. Patterson, Phys. Rev. **56**, 978 (1939).
21. Z. Wang, J. E. Alaniz, W. Jang, J. E. Garay, and C. Dames, Nano Lett. **11**, 2206 (2011).
22. L. J. Shawklein, S. J. Burns, and S. D. Jacobs, Appl. Opt. **32**, 3925 (1993).
23. ISO, "Lasers and laser-related equipment-determination of laser-induced damage threshold of optical surfaces-part 1:1-on-1 test," ISO 11254-1 (2000).
24. K. Yoshida, T. Yabe, H. Yoshida, and C. Yamanaka, J. Appl. Phys, **60**, 1545 (1986).
25. T.-T. Tan, B.-J. Liu, Z.-H. Wu, and Z.-T. Liu, Acta. Metall. Sin. **30**, 75 (2017).